

Image Registration for Prostate MR Spectroscopy Using Biomechanical Modeling and Optimization of Force and Stiffness Parameters

Ron Alterovitz¹, Ken Goldberg^{1,2}, John Kurhanewicz³, Jean Pouliot⁴, I-Chow Hsu⁴

¹Department of Industrial Engineering & Operations Research, University of California, Berkeley, CA, USA

²Department of Electrical Engineering & Computer Science, University of California, Berkeley, CA, USA

³Magnetic Resonance Science Center, University of California, San Francisco, CA, USA

⁴Department of Radiation Oncology, University of California, San Francisco, CA, USA

Abstract—We develop an image registration system based on biomechanical modeling of the prostate and surrounding tissues to register cancerous tumor locations for targeted prostate brachytherapy treatment planning. Cancerous tumors can be identified using magnetic resonance spectroscopy (MRS) imaging, which is acquired with an endorectal probe that causes significant nonlinear deformation of the prostate. The probe is removed during magnetic resonance (MR) imaging for brachytherapy planning and therapy. Given 2-dimensional segmented MR and MRS images, our finite element based model defines a mapping between the probe-in/out images by estimating the deformation of the prostate and surrounding tissues due to endorectal probe insertion and balloon inflation. Treating uncertain patient-specific model parameters for tissue stiffness and external forces as variables, we compute a locally optimal solution to maximize image registration quality. We visualize results by applying the computed mapping to the MR image to generate a deformed MR image. We compare deformed MR images to corresponding MRS images for 5 patients and obtain an average Dice Similarity Coefficient (DSC) of 95.6% for the prostate. Using the mapping, we warp a regular spectroscopy grid from the MRS image to the probe-out MR image for use during treatment planning.

Keywords—brachytherapy, finite element model, HDR, image registration, magnetic resonance imaging, MR, MRS, optimization, prostate cancer, spectroscopy

I. INTRODUCTION

Prostate cancer kills over 30,000 Americans each year [1]. It is often treated with brachytherapy, a minimally invasive medical procedure that places radioactive seeds in close proximity to cancerous tumors. High dose rate (HDR) brachytherapy uses a robot to move a single radioactive seed along approximately 20 catheters temporarily implanted inside the prostate. By adjusting the length of time (dwell time) that the seed remains at any location (dwell position) within a catheter, it is possible to generate and optimize over a wide variety of dose distributions [2].

The first step to create a targeted dose distribution is to precisely locate cancerous tumors in magnetic resonance (MR) images. Magnetic resonance spectroscopy (MRS) imaging has been effectively used to diagnose and locate cancerous tumors in the prostate [3, 4]. MRS imaging can

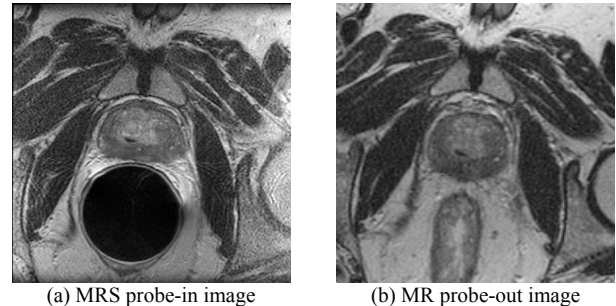


Fig. 1. Spectroscopy data is obtained when the rectal balloon is inserted and inflated (a). HDR treatment is performed with the probe removed (b).

be used to measure choline and citrate levels, which increase and decrease, respectively, with prostate cancer. To measure the low concentrations of choline and citrate, a probe containing an acquisition coil must be inserted endorectally to obtain sufficient sensitivity. The probe causes significant nonlinear translation and distortion of the prostate. The probe is removed during imaging for HDR treatment planning and therapy as shown in Fig. 1.

To register MRS probe-in images to MR probe-out images, we develop a finite element based model that estimates the deformation of the prostate and surrounding tissues in the plane of the image due to the insertion and inflation of an endorectal probe balloon. A key problem with any biomechanical model is that required patient-specific model parameters are not known, including tissue stiffness properties for the prostate central gland, peripheral zone, and surrounding tissues. Additional unknown parameters include forces due to patient position changes, bladder volume changes, and other factors that differ between the MR and MRS images but are not explicitly included in our linear elasticity soft tissue deformation model. We use an optimization algorithm to solve for locally optimal patient-specific tissue stiffness properties and external forces that maximize image registration quality. The computed deformations result in a nonlinear warping of the spectroscopy grid, as shown in Fig. 3.

II. RELATED WORK

Past work on image registration of prostate deformations includes registering treatment and interventional MR images

[5, 6] and rectal balloon probe-in/probe-out MR image registration [7, 8]. Bharatha et al. and Crouch et al. both use linear elasticity finite element models [5, 7], which require image segmentation (to specify tissue specific material properties) and mesh generation. Bharatha et al. use a tetrahedral mesh with distinct prostate central gland and peripheral zone regions while Crouch et al. generate a hexahedral mesh using a medially-based solid representation with uniform tissue properties inside the prostate. Both methods compute full 3D deformations. Unlike our method, they ignore the prostate's connectivity to surrounding tissue and rectum shape due to probe insertion.

Fei et al. develop a method that maximizes the mutual information (MI) and correlation coefficient (CC) of the image intensity histograms using rigid body translation and rotation [6]. Wu et al. develop a hybrid method for registering MR images with rectal balloons at different levels of inflation [8]. They maximize an objective function containing a weighted sum of MI and regularization energy from a non-finite element physically based model. A key advantage of MI and CC quality metrics is that tissue segmentation is not required, but these methods require long computation times (18-22 minutes for Wu et al.) and have potentially larger error due to irregular boundaries of soft tissues [6]. These metrics cannot be directly applied to our problem of registering a probe-in MRS image to a probe-out MR image because, without segmentation, the MR image contains no information on the probe insertion location.

Biomechanical image registration methods require tissue material properties as input. In past work we are aware of, these properties are either fixed as constants for all patients [5, 7] or implicitly held constant across an entire image [8]. We vary tissue stiffness values by patient and tissue type to maximize the quality of image registration. We also explicitly warp spectroscopy grids using our deformation model.

III. METHOD

Our deformable tissue registration method defines a mapping between a probe-in MRS image and a probe-out MR image. At the core of our method is a finite element model that estimates the deformation of soft tissues in the MR image due to insertion and inflation of the rectal probe balloon. Treating the unknown stiffness properties and external forces as variables, we compute a local optimal solution that maximizes image registration quality. Our current optimization includes 3 unknown stiffness parameters and between 20 and 40 external forces applied on the prostate boundary, each with 2 degrees of freedom.

A. Method Input

The input for our image registration method is a probe-out MR image and a probe-in MRS image with the rectum and prostate manually segmented using polygonal

boundaries. We assume the MR and MRS images are in the same plane and rigid points, such as points in bones, are manually aligned. For improved accuracy, we also segment bones and separately segment the prostate central gland (CG) and peripheral zone (PZ) in the probe-out MR image.

B. Finite Element Model of Soft Tissue Deformations

We approximate tissues as nearly incompressible (Poisson's ratio of 0.49), linearly elastic, and isotropic. Although tissue stiffness properties will be modified during the optimization method, initial default values must be set. Based on biomechanics literature for tissue stiffness measurements, we assign a Young's modulus of 60kPa to the prostate and 30kPa to all surrounding tissues [9]. We assume initial external force magnitudes are 0.

Based on the polygonal segmentation boundaries, we automatically generate a finite element mesh composed of $n=500$ nodes and between 800 and 1,000 triangular elements using the constrained Delaunay triangulation software program Triangle [10]. Elements are assigned default stiffness properties based on tissue type. Mesh nodes defining elements inside bones are constrained to be fixed.

As shown in Fig. 2, our model inflates the rectum in the MR image to match the rectum outline in the MRS image. We project MR image mesh nodes along the ray based at the rectum center and constrain them to the intersection with the MRS image rectum outline. The deformations of the surrounding soft tissues, including the prostate, are computed using a finite element method (FEM).

The FEM problem for a given MR image mesh with n nodes is defined by a system $\mathbf{K} \mathbf{u} = \mathbf{f}$ containing $2n$ linear equations where \mathbf{K} is the global stiffness matrix, \mathbf{f} is the external force vector, and \mathbf{u} is the nodal displacement vector [11]. For each fixed node, we remove its 2 corresponding equations from the system. We solve the linear system of equations numerically using the Gauss-Seidel method to compute nodal displacements \mathbf{u} for non-fixed nodes. Using linear interpolation within each element of the mesh, the nodal displacement vector \mathbf{u} defines a complete bidirectional mapping function F between the MR image and the corresponding MRS image. Mapping F is applied to every pixel in the MR image to obtain the deformed MR image. The quality of the mapping F is determined by how closely the deformed MR image matches the MRS image.

C. Quality Metric

To quantify the accuracy of the image registration, we measure the overlap between prostate area in the MRS image and the prostate area in the deformed MR image. Given outlined areas in two images, the Dice Similarity Coefficient (DSC) is defined as:

$$D = \frac{2a}{2a + b + c}$$

where a is the number of picture elements (pixels) shared by both areas, b is the number of pixels unique to the first area,

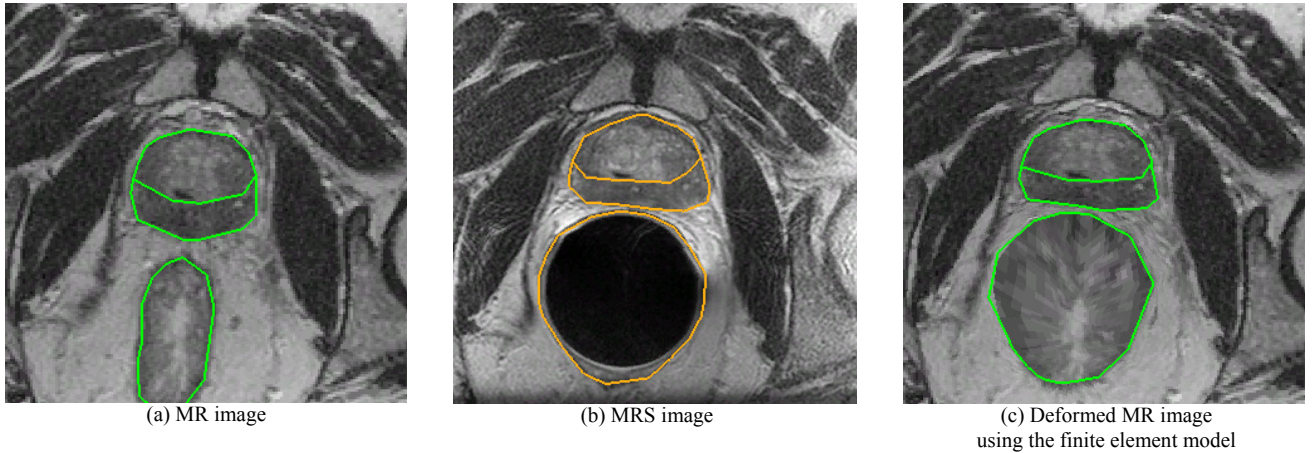


Fig. 2: The prostate central gland, peripheral zone, and rectum are outlined in the probe-out MR image (a) and the corresponding probe-in MRS image (b). The output of our method (c) displaces mesh nodes along the rectum in the MR image to the rectum outline in the MRS image and estimates the resulting soft tissue deformations. The image registration quality for (b) and (c) is $D = 97.8\%$.

and c is the number of pixels unique to the second area [12, 5]. The DSC is a scalar between 0 and 1, with higher values representing better quality registration.

D. Optimization of Uncertain Parameters

Our image registration method treats tissue stiffness properties and external forces at mesh nodes along the prostate boundary as unknown variables. Tissue stiffness is constrained between 1kPa and 600kPa. External force magnitudes are unbounded. We define the optimization objective function for maximization as:

$$Q = D - \alpha E$$

where D is the DSC for the prostate total gland, α is a scaling parameter, and E is the percent of strain energy due to external forces. We subtract E in the objective function to prioritize optimization of parameters of the physically-based model (tissue stiffness) and minimize dependence on external forces. This produces visually smoother image mappings by preventing unrealistic large magnitude external forces. Based on our trials, $\alpha=0.005$ produced best results.

We use the Steepest Descent method with Armijo's Rule for line search to maximize the nonlinear objective function Q [13]. The variables, which include $m=3$ tissue stiffness properties and $l \approx 60$ external force degrees of freedom depending on the mesh, are defined in a vector \mathbf{x} of dimension $m+l$. The quality metric Q is a function $Q(\mathbf{x})$. We numerically compute derivatives for the gradient $\nabla Q(\mathbf{x})$ using finite differences. At iteration i of the Steepest Descent optimization method, Armijo's Rule selects the next candidate point $\mathbf{x}_{i+1} = \mathbf{x}_i + 2^t \lambda \nabla Q(\mathbf{x}_i)$ for predefined step size λ by sequentially incrementing integer t starting at $t=0$ to solve for the maximum t such that $Q(\mathbf{x}_{i+1}) > Q(\mathbf{x}_i)$. Then the gradient $\nabla Q(\mathbf{x}_{i+1})$ is computed and the algorithm repeats until iteration j where $\|\nabla Q(\mathbf{x}_j)\| < \epsilon$, $\epsilon = 0.001$. This method converges linearly to a local optimal solution [13].

E. Warping the Spectroscopy Grid

MR spectroscopic data is collected inside voxels defined by a regular 7mm grid. To help register spectroscopic data to the probe-out MR image, we transform each intersection point in the spectroscopy grid from the MRS image to the probe-out MR image using mapping F defined in III.B.

IV. RESULTS

To visualize the predicted tissue deformations, we texture map triangles using node positions from the original probe-out mesh as texture coordinates and node locations from the deformed probe-out mesh as object coordinates. As shown in Fig. 2(c), the deformed MR image closely matches the probe-in MRS image in Fig. 2(b). The resulting warping of the spectroscopy grid from the MRS image to the probe-out MR image is clearly nonlinear, as shown in Fig. 3(c).

We tested the image registration method on MR/MRS image slices from 5 patients. The mean DSC for the prostate for deformed MR images was 95.6% with a standard deviation of 1.3%. The registration algorithm required an average of 27.8 seconds with a standard deviation of 17.6 seconds to complete on a 1.6GHz Pentium-M laptop PC. The strain energy percentage due to external forces E averaged 7.7%.

TABLE I:

DSC QUALITY METRIC AND STANDARD DEVIATIONS (IN PARENTHESES) FOR PATIENT MR/MRS IMAGES

	Rigid Registration	Deformable Tissue Registration
Central gland DSC	90.6% (2.8%)	94.9% (0.4%)
Peripheral zone DSC	73.2% (14.4%)	80.6% (19.2%)
Total gland DSC	84.8% (14.1%)	95.6% (1.3%)

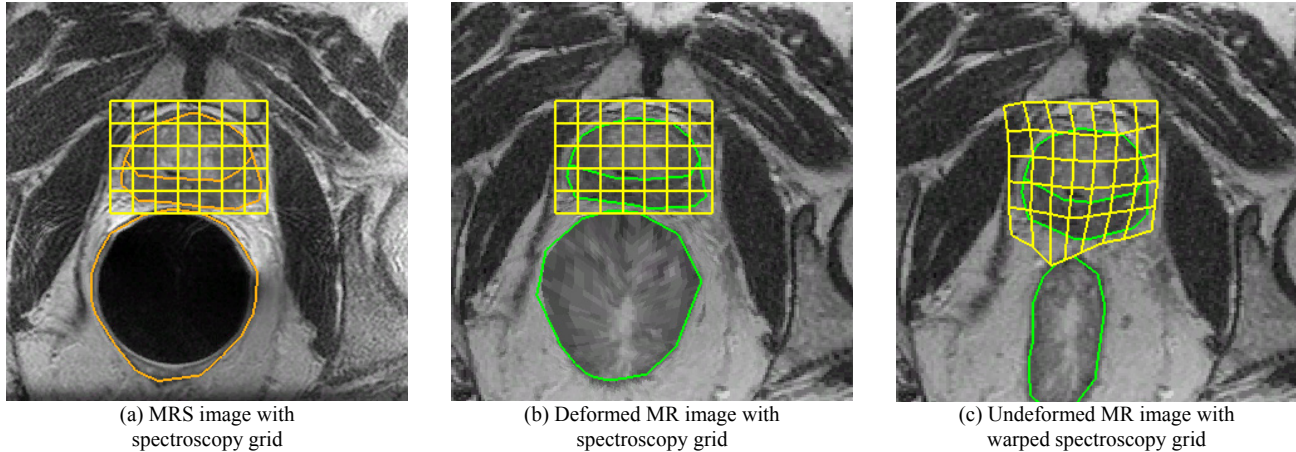


Fig. 3. A comparison of MRS and MR images shows the nonlinear warping of the spectroscopy grid. The MRS image (a) closely matches the computed deformed MR image (b) outside the inflated balloon. The spectroscopy grid is warped to the undeformed MR image (c) for use during treatment planning.

We compare our deformable tissue registration method to a center of mass rigid registration method where the prostate total gland is translated in the MR image by the distance between its center of mass in the MR and MRS images [5]. In addition to registering the prostate total gland for 5 patients, we also manually segmented the CG and PZ in the MRS images for 3 patients to measure DSC errors for these areas, although this boundary is not always well defined and is subject to significant segmentation error. Our deformable tissue registration method generated significantly better results for the tested images, as shown in TABLE I.

V. CONCLUSION AND FUTURE WORK

The endorectal probe employed during prostate MR spectroscopy causes significant deformations to the prostate and surrounding tissue which can be estimated using our deformable tissue image registration method. The method requires on average under 30 seconds of computation time on a 1.6GHz Pentium-M laptop PC to estimate tissue deformations and produce a nonlinear probe-in/out image mapping with an average DSC quality of 95.6%.

We plan to improve our biomechanical model of tissue deformation to more accurately predict soft tissue deformations due to rectal probe insertion. This will include incorporating anisotropic nonlinear tissue properties into the optimization framework and investigating appropriate friction/slip conditions around the balloon and between the prostate and surrounding tissues. We also plan to extend our planar model to a 3D volumetric model and to implement and evaluate new quality metrics and optimization methods.

ACKNOWLEDGEMENT

We thank Michael Yu for his programming help and Yongbok Kim, Sue Noworolski, Dezhen Song, and K. Gopalakrishnan for their advice and feedback. We also

thank the National Science Foundation Graduate Research Fellowship program for their financial support.

REFERENCES

- [1] National Center for Health Statistics, "Prostate disease." Available: <http://www.cdc.gov/nchs/fastats/prostate.htm>
- [2] E. Lessard and J. Pouliot, "Inverse planning anatomy-based dose optimization for HDR-brachytherapy of the prostate using fast simulated annealing algorithm and dedicated objective function," *Med. Phys.*, vol. 28, no. 5, pp. 773-779, May 2001.
- [3] J. Kurhanewicz, H. Hricak, D. B. Vigneron, et al., "Prostate cancer: Metabolic response to cryosurgery as detected with 3D H-1 MR spectroscopic imaging," *Radiology*, vol. 200, no. 2, pp. 489-496, 1996.
- [4] J. Kurhanewicz, D.B. Vigneron, H. Hricak, et al., "Three-dimensional H-1 MR spectroscopic imaging of the in situ human prostate with high (0.24-0.7-cm³) spatial resolution," *Radiology*, vol. 198, no. 3, pp. 795-805, 1996.
- [5] A. Bharatha, M. Hirose, N. Hata, S. K. Warfield, M. Ferrant, K. H. Zou, E. Suarez-Santana, J. Ruiz-Alzola, A. D'Amico, R. A. Cormack, R. Kikinis, F. A. Jolesz, and C. M. C. Tempany, "Evaluation of three-dimensional finite element-based deformable registration of pre- and intraoperative prostate imaging," *Med. Phys.*, vol. 28, no. 12, pp. 2551-2560, Dec. 2001.
- [6] B. Fei, A. Wheaton, Z. Lee, J. I. Duerk, and D. Wilson, "Automatic MR volume registration and its evaluation for the pelvis and prostate," *Phys. Med. Biol.*, vol. 47, no. 5, pp. 823-38, Mar. 2002.
- [7] J. R. Crouch, S. M. Pizer, E. L. Chaney, and M. Zaider, "Medially based meshing with finite element analysis of prostate deformation," *Med. Imag. Com. and Comp. Ass. Int. (MICCAI)*, pp. 108-115, 2003.
- [8] X. Wu, S. J. Dibiase, R. Gullapalli, and C. X. Yu, "Deformable image registration for the use of Magnetic Resonance Spectroscopy in prostate treatment planning," *Int. J. Radiation Oncology Biol. Phys.*, vol. 58, no. 5, pp. 1577-1583, 2004.
- [9] T. A. Krouskop, T. M. Wheeler, F. Kallel, B. S. Garria, and T. Hall, "Elastic moduli of breast and prostate tissues under compression," *Ultrasonic Imaging*, vol. 20, no. 4, pp. 260-274, Oct. 1998.
- [10] J. Shewchuk, "Triangle: A two-dimensional quality mesh generator and Delaunay triangulator." Available: <http://www-2.cs.cmu.edu/~quake/triangle.html>
- [11] O. C. Zienkiewicz and R.L. Taylor, *The Finite Element Method*, Fifth Edition, Butterworth-Heinemann, 2000.
- [12] L. R. Dice, "Measures of the amount of ecologic association between species," *Ecology*, vol. 26, no. 3, pp. 297-302, 1945.
- [13] M. S. Bazaraa, H. D. Sherali, and C. M. Shetty, *Nonlinear Programming: Theory and Algorithms*, Second Edition, John Wiley & Sons, Inc., 1993.